# Multi-Angle Remote Sensing of Cumulus Geometry

*E. I. Kassianov*
*Pacific Northwest National Laboratory*
*Richland, Washington*
*and*
*Institute of Atmospheric Optics*
*Tomsk, Russia*

*T. P. Ackerman and R. T. Marchand*
*Pacific Northwest National Laboratory*
*Richland, Washington*

## Introduction

Satellite remote sensing is the major source for statistics of cloud properties; however, accurate and robust methods for extracting both optical and geometrical characteristics of broken clouds have yet to be fully developed. Currently, most broken cloud retrieval schemes rely on spectral (e.g., microwave, visible, or infrared [IR]) observations from near-vertically pointing remote sensors (Rossow 1989; Minnis et al. 1992). Although the multi-spectral techniques can provide accurate retrievals of cloud fraction and mean optical depth, the estimation of other important parameters, such as cloud vertical thickness, are not as reliable.

In this paper, we demonstrate how the horizontal distribution of cloud pixels and their vertical geometrical thickness can be reconstructed from multi-angle satellite observations. Physically, the suggested approach is based on two obvious dependences: (1) for a fixed horizontal cloud distribution, the probability of a clear line of sight is a monotonically decreasing function of zenith viewing angle, and (2) the decrease rate of this probability depends on the vertical cloud size stratification. The study is focused on the special case of small marine cumulus clouds observed by the multi-angle imaging spectroradiometer (MISR), recently launched on the National Aeronautics and Space Administration (NASA) Terra platform.

## Directional and Average Cloud Fraction

Among fundamental parameters describing the geometry of broken clouds is the directional cloud fraction, $N(\theta) = 1 - P_{clear}(\theta)$, where $P_{clear}(\theta)$ is the probability of a clear line of sight at zenith viewing angle $\theta$. The directional cloud fraction $N(\theta)$ depends on the nadir-view cloud fraction $N_{nadir}$, the horizontal cloud distribution (e.g., random, clustered, or regular), and vertical cloud size variability. In the general case, an empirical expression for $N(\theta)$ can be formulated based on field data or results of model simulations. For some cloud models, an analytical expression can be obtained in terms of cloud bulk geometrical parameters (Han and Ellingson 1999; Titov 1990). As an example, for a broken cloud

field composed of randomly placed parallelepipeds with identical and constant geometrical thickness $\Delta h$, the directional cloud fraction is given by (Titov 1990)

$$N(\theta) = 1 - P_{clear}(\theta) = 1 - (1 - N_{nadir}) \times \exp\left\{ - \frac{\rho \, \Delta h \, \tan\theta}{D} \right\} \qquad (1)$$

where $\rho$ and $D$ are the model parameter and the average horizontal cloud size, respectively. From Eq. (1) it follows that $N_{nadir}$, $D$, and $\Delta h$ can be determined uniquely by high-resolution observations from nadir and oblique (off-nadir) viewing directions. The geometrical thickness $\Delta h$ of broken clouds can vary strongly in space, so that the directional cloud fraction $N(\theta)$ may be dependent not only on the first moment (the average vertical cloud size $\Delta H$), but also on higher statistical moments describing the $\Delta h$ variations.

The following simple example shows qualitatively how variations of cloud top height influence the directional cloud fraction $N(\theta)$. We consider a two-dimensional cloud (a cloud infinite in the y-direction), assuming that the cloud consists of just three pixels with the same horizontal size $L$ (cloud horizontal size is $D = 3 \times L$) and the same cloud base $Hb$ ($Hb = 0$). Let us consider two cases. For case 1, all pixels have the same vertical size $H$. For case 2, the first and third pixels have the same vertical size $h_{\min} = H/2$, while the vertical size of the second (middle) pixel is $h_{\max} = 2 \times H$. Obviously, both case 1 and case 2 have identical mean vertical size $H$. From simple geometrical considerations, it follows that, for slant viewing directions, the directional cloud fraction $N(\theta)$ (cloud projection onto x-axis) will be $D + H \times \tan(\theta)$ for the case 1; while for case 2, the size of the geometrical shadow will be $D + h_{\min} \times \tan(\theta)$ if $(h_{\max} - h_{\min}) \times \tan(\theta) \le L$ and $D - L + h_{\min} \times \tan(\theta)$ if $(h_{\max} - h_{\min}) \times \tan(\theta) > L$. Thus, for the same horizontal $D$ and mean vertical $H$ cloud sizes, the directional cloud fraction $N(\theta)$, corresponding to the case with irregular cloud top boundary (case 2), can either be greater or less than the directional cloud fraction $N(\theta)$, corresponding to the case with plane parallel cloud geometry (case 1). For a cloud field, the dependence of $N(\theta)$ on cloud shape will be even more complex, because of the effects of mutual cloud shadowing. These effects, in turn, depend on the horizontal cloud distribution and vertical cloud structure.

For accurate $\Delta h$ retrieval, data for nadir and oblique viewing angles must be available. High-resolution ($\Delta x \sim 0.275$ km) observations at nine viewing angles ($\theta_1 = -70.5$, $\theta_2 = -60$, $\theta_3 = -45.6$, $\theta_4 = -26.1$, $\theta_5 = 0$, $\theta_6 = 26.1$, $\theta_7 = 45.6$, $\theta_8 = 60$, $\theta_9 = 70.5$) are available from the MISR, recently launched on the NASA Terra platform. From here on, forward ($\phi$=0) zenith angles are positive, while aft ($\phi$=180) ones are negative. Also, we have $N_{nadir} = N(\theta_5)$. Because the MISR instrument measures reflectance in nine viewing directions, it seems reasonable to use all this information for $\Delta h$ retrieval. To do that, we introduce an *average* cloud fraction $N_{avr}$ defined as:

$$N_{avr} = \frac{1}{n} \sum_{i=1}^{n} N(\theta_i), \qquad n = 9 \qquad (2)$$

We now discuss how $N(\theta)$ can be retrieved from satellite data.

## Average Cloud Fraction and Threshold

Given a set of measured reflectances at a single angle $I(\theta)$, a corresponding probability density function $pdf\{I(\theta)\}$can readily be obtained that satisfies the normalization condition

$$\int_{I_{\min}(\theta)}^{I_{\max}(\theta)} pdf\{I(\theta)\}dI(\theta) = 1, \quad (3)$$

where $I_{\min}(\theta)$ and $I_{\max}(\theta)$ are the minimum and maximum reflectances, respectively.

One can define the directional cloud fraction $N_{obs}(\theta)$ as:

$$N_{obs}(\theta) = \int_{I_0(\theta)}^{I_{\max}(\theta)} pdf\{I(\theta)\}dI(\theta), \quad (4)$$

where $I_0(\theta)$is a radiative threshold.

Here and below, the subscript "*obs*" on $N(\theta)$ and other variables indicates that they are obtained on the basis of Eq. (4). We emphasize, that the threshold $I_0(\theta)$ depends on cloud geometrical and optical properties, atmospheric and surface parameters, and illumination conditions (solar zenith and azimuth angles). Presently, no reliable methods are available to select a threshold set $I_0(\theta) = \{I_0(\theta_i), i = 1, ..., 9\}$ unambiguously; hence, the use of $N_{avr,obs}$ for a $\Delta h$ retrieval is not generally justified.

We consider an alternative parameter

$$\Delta N = N_{avr} - N_{nadir}. \quad (5)$$

For a fixed horizontal distribution of cloud pixels, the parameter $\Delta N_{obs}$ characterizes the relative influence of their vertical geometrical thickness $\Delta h$ on $N_{avr,obs}$. Obviously, the $\Delta h$ retrievals should use $\Delta N_{obs}$ values as large as possible, in order to get the maximum effect of $\Delta h$. According to Eqs. (2) and (4), $\Delta N_{obs}$ is a function of nine parameters $I_0(\theta_i)$, $i = 1, ..., 9$. For simpler presentation and easier comparison of results, a change to a *single* relative variable is useful. To perform a calculation of $I=N_{obs}(\theta_i)$, $i = 1, ..., 9$, steps (bins) $\Delta I(\theta_i) = [I_{\max}(\theta_i) - I_{\min}(\theta_i)] / M$, were selected. The parameter $M$, which will be referred to as the number of intensity bins, was set to be equal for all $\theta_i$, i = 1, ..., 9. In this case, $I_0(\theta_i) = I_{\min}(\theta_i) + m \times \Delta I(\theta_i)$, i = 1, ..., 9 and $\Delta N_{obs}$ depends on just *one* relative variable (digital count) $m$, $m = 1, ..., M$.

The $\Delta h$ retrieval algorithm proposed here consists of the following steps:

- A relative value $m = m^*$ is determined, at which $\Delta N_{obs}(m^*)$ peaks.

- An absolute threshold is selected for nadir radiance: $I_0^*(\theta_5) = I_{\min}(\theta_5) + \Delta I(\theta_5) \times m^*$. This value $I_0^*(\theta_5)$ is then used for determining horizontal cloud distribution. Specifically, the condition $I(\theta_5) > I_0^*(\theta_5)$ is checked for each pixel. All pixels satisfying this condition are flagged as 100% cloud coverage, all other pixels are background (clear-sky).

- For the fixed horizontal distribution of clouds, the parameters of the chosen cloud model are adjusted such that $\Delta N_{\text{mod}} = \Delta N_{obs}(m^*)$.

# MISR Data and Cloud Retrieval

In the following example, only eight MISR images (~15x15 km$^2$), representing a field of small ($D$~1 km) marine cumulus off the coast of California, have been considered because the *Aa* camera ($\theta_4$ = -26.1) was not working properly during this orbit. These eight MISR images were processed to obtain the corresponding radiance probability densities *pdf* {$I$} as functions of the dimensionless digital count $m$, and these quantities were then used to calculate the nadir-view $N_{nadir,obs}$ and average $N_{avr,obs}$ cloud fractions (Figure 1). In contrast to $N_{nadir,obs}$ and $N_{avr,obs}$, the difference $\Delta N_{obs}$ is not a monotonically decreasing function of $m$ and has a maximum $\Delta N_{obs}$ = 0.133 at $m$ = 14 (Figure 1). Correspondingly, the absolute nadir radiance $I(\theta_5)$ at $m$ = 14 is 15.7 (radiance dimension is $Wm^{-2}\ sr^{-1}\ \mu m^{-1}$). This value $I(\theta_5)$ = 15.7 was used here as a threshold $I_0(\theta_5)$. It should be noted that the threshold values representing more than 3% minimum visible reflectivity (clear sky) have been frequently used for cloud detection (Rossow et al. 1985). The selection of threshold $I_0(\theta_5)$ and, thereby, designation of the horizontal distribution of cloud pixels conclude the first step of the $\Delta h$ retrieval.

Next, for determining $\Delta N_{\text{mod}}$, we need to select a cloud model. In other words, we have to establish a rule by which to determine the geometrical thickness of each cloud pixel. A model that relates the geometrical $\Delta h$ and optical thickness, $\tau$, of the cloudy pixels has been suggested (Minnis et al. 1992). The optical thickness can be determined by the independent pixel approximation (IPA), whose accuracy degrades with increasing horizontal inhomogeneity of the cloud field and/or increasing horizontal resolution of cloud observations (Chambers et al. 1997). The cloud field considered here is highly inhomogeneous in the horizontal; therefore, the use of the IPA for an accurate $\Delta h$ retrieval with high spatial resolution ($\Delta$x~0.275 km) would be problematic.

### Cloud Model Specification

The cloud model used here was chosen based on the following general considerations. First, geometrically thick pixels typically have a large nadir reflectance, but for geometrically thin pixels, the reverse is true. Further, the nadir radiance depends nonlinearly on the geometrical thickness. At our initial exploratory stage, it is reasonable to use a simple expression to approximate this unknown nonlinear dependence. The sensitivity of the $\Delta h$ retrieval to the choice of the cloud model can be best evaluated using cloud models differing by as much as possible. We chose to use the following two models.

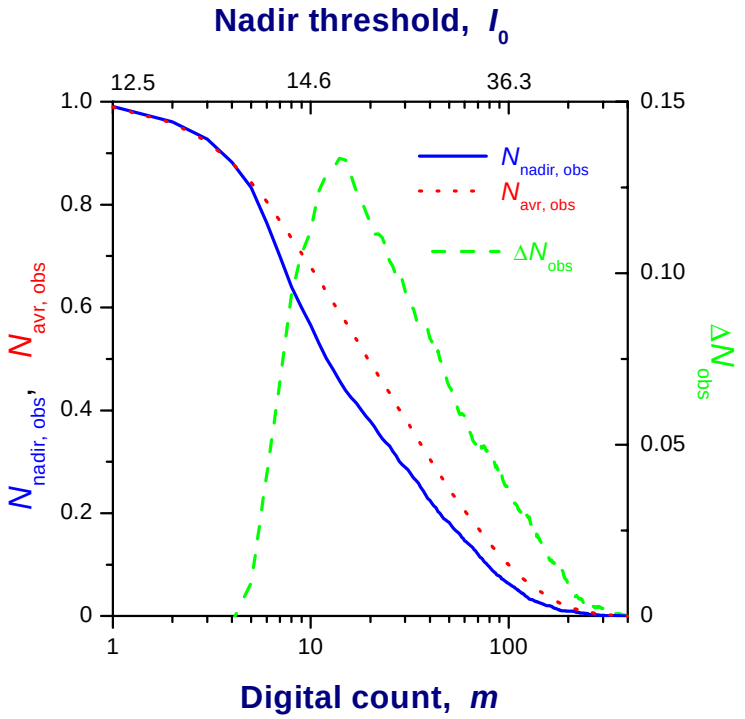


**Figure 1**. The nadir-view $N_{nadir,obs}$, average $N_{avr,obs}$ cloud fractions and their difference $\Delta N_{obs} = N_{avr,obs} - N_{nadir,obs}$ as functions of digital count $m$. A scale converting $m$ to equivalent nadir threshold $I_0(\theta_5)$ is given at the top of the figure.

*Model 1*. For each cloud pixel, the vertical cloud height was taken to be proportional to the nadir radiance $I(\theta_5)$ and its square root:

$$\Delta h_{\mathrm{mod},1} = a_1 + b_1 \times I(\theta_5) + c_1 \times \sqrt{I(\theta_5)} \qquad (6a)$$

*Model 2*. For each cloud pixel, the vertical cloud height was taken to be proportional to the natural logarithm of the nadir radiance $I(\theta_5)$:

$$\Delta h_{\mathrm{mod},2} = a_2 + b_2 \times \ln\{I(\theta_5)\}. \qquad (6b)$$

The coefficients in both models are obtained by fitting the model to the observations as described in the next section. A set of coefficients is found for each assumed average geometrical thickness.

An example of the probability distributions, $pdf\{\Delta h_{\mathrm{mod}}\}$, corresponding to these two models, is presented in Figure 2. As seen, these models differ significantly: the distribution $pdf\{\Delta h_{\mathrm{mod},1}\}$ is approximately three times wider than $pdf\{\Delta h_{\mathrm{mod},2}\}$. Both of these models give physically meaningful

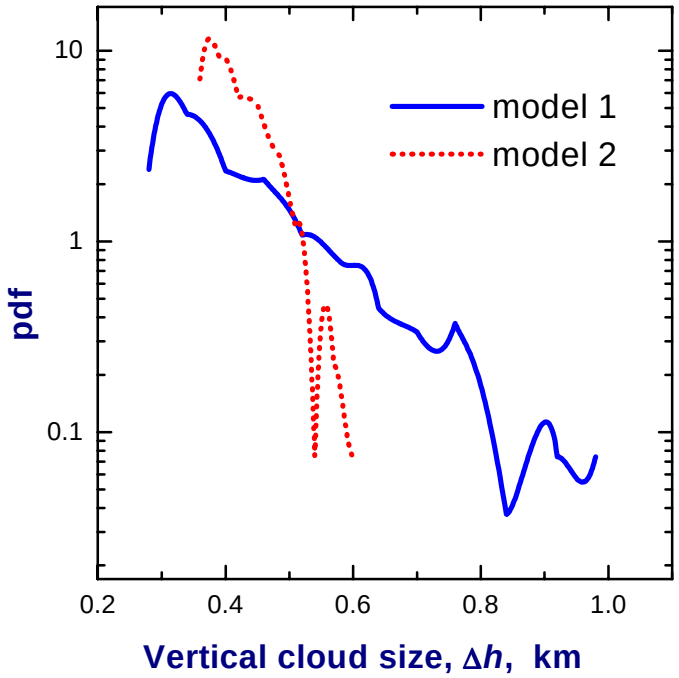


**Figure 2**. Probability density functions of the cloud geometrical thickness $\Delta h_{mod}$, corresponding to the different models. Both model distributions $\Delta h_{mod,1}$ and $\Delta h_{mod,2}$ have the same average value $\Delta H_{mod}$ = 0.42 km. The model geometrical thicknesses $\Delta h_{mod,1}$ and $\Delta h_{mod,2}$ are obtained from Eqs. (6a) and (6b) at particular values $a_1$ = 0.01, $b_1$ = 0.01, $c_1$ = 0.03, and $a_2$ = 0, $b_2$ = 0.13.

results (Figure 3). In particular, large clouds, on average, have larger vertical extent, and the largest (smallest) possible $\Delta h_{mod}$ values typically occur in the central portion (near the edge) of these clouds (Figures 3 and 4). Smaller clouds, correspondingly, have less mean vertical extent. The variation of $\Delta h_{mod}$ within small clouds is insignificant. Since model 2 has a narrower distribution $pdf\{\Delta h_{mod,2}\}$, the amplitude of fluctuations of the geometrical thickness $\Delta h_{mod,2}$ is much less than that of $\Delta h_{mod,1}$ (Figures 3 and 4). On average, the inequality $\Delta h_{mod,2} > \Delta h_{mod,1}$ occurs for small clouds, and the opposite is true for large clouds. Also, for model 2, clouds have a less "convex" appearance, because the distribution of $\Delta h_{mod,2}$ within clouds is more uniform. Consequently, the use of a different cloud model will introduce differences between (i) the mean vertical extents of small and large clouds (the amplitude of fluctuations) and (ii) cloud shapes (more or less "convex" appearance).

We now discuss the qualitative dependence of directional cloud fraction $N(\theta)$ on the choice of the cloud model. The studied cloud field can be conventionally segregated into small and large clouds. The directional cloud fraction $N(\theta)$ can also be divided into three terms: $N1(\theta) + N2(\theta) + N3(\theta)$. The first term $N1(\theta)$characterizes the contribution of small clouds to the directional cloud fraction. The second term $N2(\theta)$ quantifies the contribution of large clouds to $N(\theta)$. The third term $N3(\theta)$ accounts for the effects of mutual cloud shadowing and their contribution to $N(\theta)$. Obviously, in the nadir direction, the effects of mutual cloud shadowing are absent, that is $N3(\theta) = 0$. The value of $N3(\theta)$ depends not only on the vertical distribution of clouds, but also on how they are distributed in horizontal. Recall that the

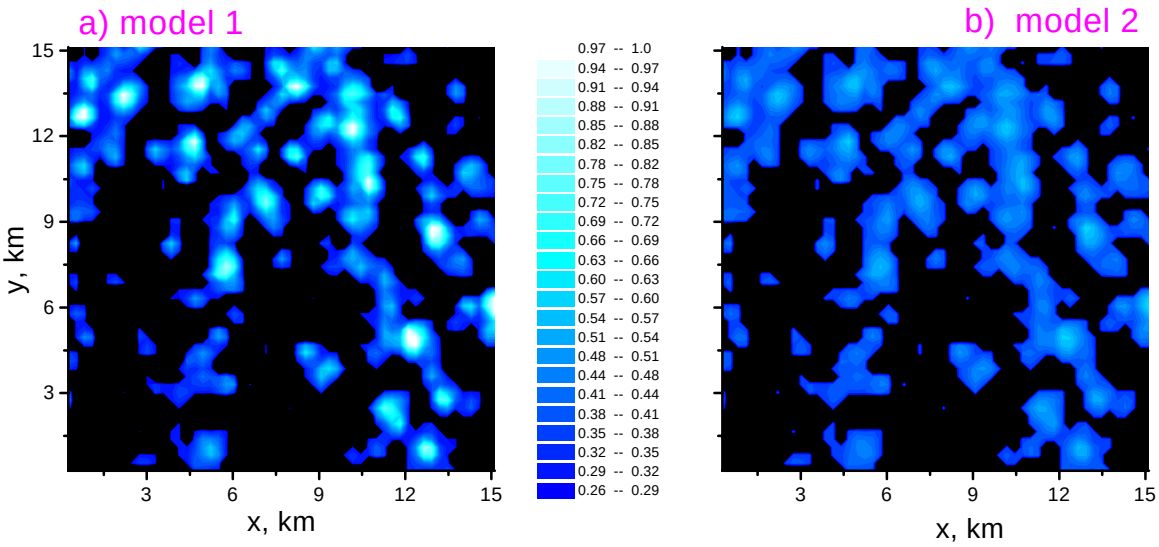


**Figure 3**. Horizontal distribution of cloud pixels for digital count $m^*$ = 14 (nadir radiance threshold $I(\theta_5)$ = 15.7. For a given value of $m = m^*$ the absolute cloud fraction $N_{obs}(m^*)$ is equal to 0.457. The model geometrical thicknesses $\Delta h_{mod,1}$ and $\Delta h_{mod,2}$ have probability distribution functions (pdf) presented in Figure 2.

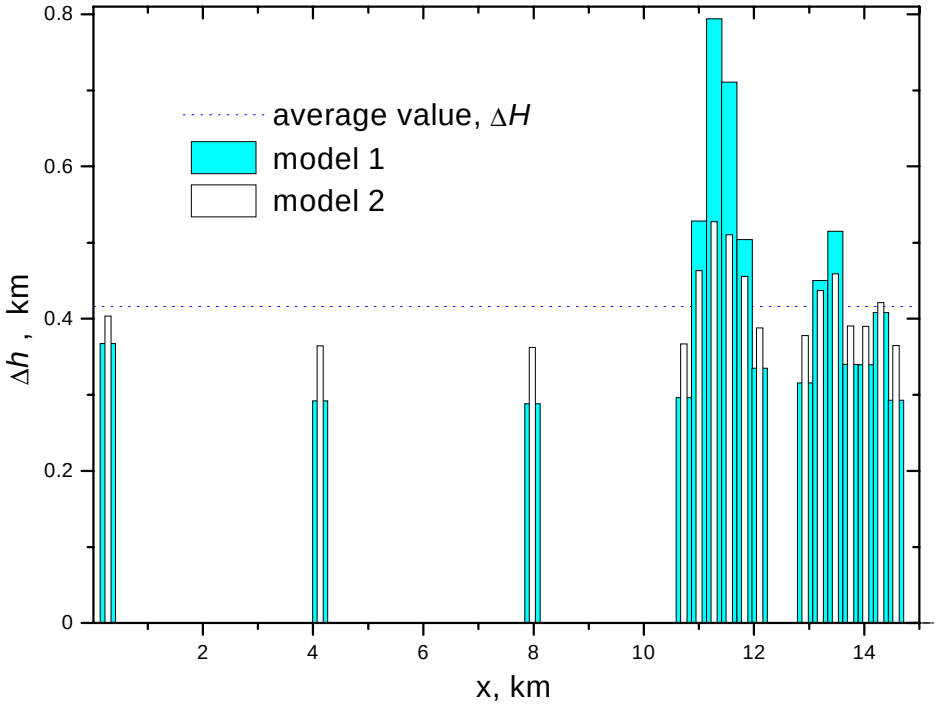


**Figure 4**. Vertical cross-section of (y = 2.5 km) of two cloud fields shown in Figure 3.

models have an identical horizontal distribution. For both model 1 and model 2 small clouds have an almost uniform cloud top. Small clouds in model 1 have less geometrical thickness and therefore, on average, the inequality $N1_{\mathrm{mod},1}(\theta) < N1_{\mathrm{mod},2}(\theta)$ holds. The second term $N2(\theta)$ depends on the cloud model in a more complex way. Large clouds in model 1 have larger geometrical thickness and more "convex" appearance. For small $\Delta H$ and small oblique viewing angles, on average, the inequality $N2_{\mathrm{mod},1}(\theta) < N2_{\mathrm{mod},2}(\theta)$ holds. For larger $\Delta H$ values and larger oblique viewing angles, the situation is opposite (see e.g., the qualitative example in the section on directional and average cloud fraction). One would expect that for small $\Delta H$, the third term $N3(\theta)$ will be small, and the inequality $N_{\mathrm{mod},1}(\theta) < N_{\mathrm{mod},2}(\theta)$ will occur. Because the directional cloud fraction $N(\theta)$ depends on the cloud models, then the average cloud fraction $N_{avr}$ and the difference $\Delta N_{\mathrm{mod}}$ also will be functions of the cloud type specification. Obviously, the differences in $\Delta N_{\mathrm{mod},1}$ and $\Delta N_{\mathrm{mod},2}$ will introduce differences in the retrieved values of $\Delta h_{\mathrm{mod},1}$ and $\Delta h_{\mathrm{mod},2}$.

## Vertical Cloud Size Retrieval

The final step of our suggested approach is to determine the model parameters $\Delta h_{\mathrm{mod}}$ for which $\Delta N_{\mathrm{mod}} = N_{obs}(m^*)$. The "tuning" of $\Delta h_{\mathrm{mod}}$ was done using a fixed horizontal distribution of cloud pixels (Figure 3). For the cloud models considered here, this was done using the following procedure. An initial vertical distribution $\Delta h^{(0)}_{\mathrm{mod},1}$, for which the average value $\Delta H^{(0)} = 0.21$ km, was specified. For the given vertical distribution, $N^{(0)}_{\mathrm{mod},1}(\theta_i)$, $i = 1, \ldots, 9$, were calculated using the Monte Carlo method. Based on these values, the difference $\Delta N^{(0)}_{\mathrm{mod},1}$=0.078 was finally determined. This procedure was repeated for three additional vertical distributions $\Delta h_{\mathrm{mod},1}$ connected with the initial one; namely, for $\Delta h^{(2)}_{\mathrm{mod},1} = 1.5 \times \Delta h^{(1)}_{\mathrm{mod},1}$, $\Delta h^{(3)}_{\mathrm{mod},1} = 2 \times \Delta h^{(1)}_{\mathrm{mod},1}$ and $\Delta h^{(4)}_{\mathrm{mod},1} = 2.5 \times \Delta h^{(1)}_{\mathrm{mod},1}$. Based on these vertical distributions, the average vertical cloud sizes $\Delta H^{(k)}$ and the differences $\Delta N^{(k)}_{\mathrm{mod},1}$ $k = 2, \ldots, 4$ were finally obtained. Thereupon, $\Delta N^{(k)}_{\mathrm{mod},1}$ versus $\Delta H^{(k)}$, k = 1, ..., 4, was plotted (Figure 5). The same steps were taken for model 2. Thereupon, $\Delta N^{(k)}_{\mathrm{mod},2}$ versus $\Delta H^{(k)}$, k = 1, ..., 4, was also plotted (Figure 5). We note that, in the given models, $\Delta N_{\mathrm{mod},1}$ and $\Delta N_{\mathrm{mod},2}$ are fairly smooth and monotonically increasing functions of the average vertical cloud size $\Delta H$. As seen, the maximum difference between $\Delta N_{\mathrm{mod},2}$ and $\Delta N_{\mathrm{mod},1}$ takes place for small $\Delta H$ values, and this difference decreases with increasing $\Delta H$. At small $\Delta H$, the relative contribution of mutual shading is small. Hence, the differences between $\Delta N_{\mathrm{mod},1}$ and $\Delta N_{\mathrm{mod},2}$ arise primarily from model 1 to model 2 differences in $\Delta h_{\mathrm{mod}}$ distributions of both small and large clouds. The qualitative dependence of these terms on each model was discussed above (cloud model specification).

The model curves were then used to retrieve $\Delta H_{obs}$ (Figure 5). The equality $\Delta N_{\mathrm{mod}} = \Delta N_{obs}$ takes place for $\Delta H_{\mathrm{mod},1}$ ~0.39 km and $\Delta H_{\mathrm{mod},2}$ ~0.34 km, correspondingly, for model 1 and model 2. The retrieved values $\Delta H$ are within physically acceptable limits. Despite the great difference between these two models (Figure 2), the values $\Delta H_{\mathrm{mod},1}$ and $\Delta H_{\mathrm{mod},2}$ differ insignificantly, by approximately 10%. Hence,

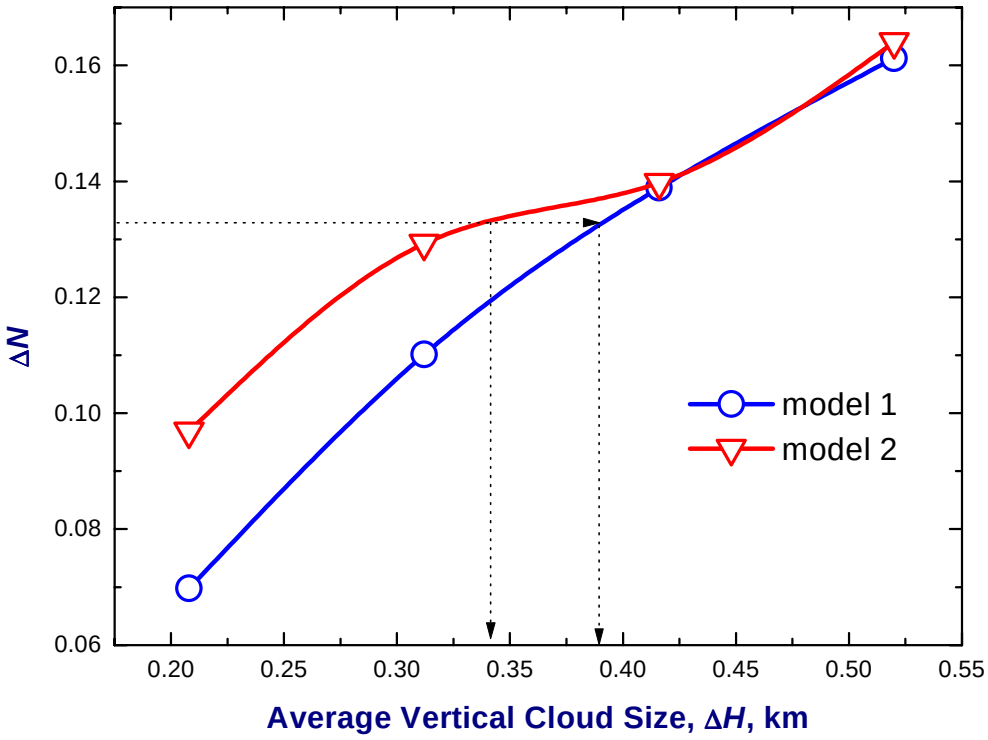


**Figure 5**. Difference $\Delta N_{mod}$ as a function of the average geometrical thickness $\Delta H_{mod}$ for two different cloud models. The values of $\Delta H_{mod,1}$ and $\Delta H_{mod,2}$ such that $\Delta N_{mod,1}$ and $\Delta N_{mod,2}$ are equal to $\Delta N_{obs}$ are shown.

we can make a preliminary conclusion that, for the given horizontal distribution of clouds, the average retrieved geometrical thickness depends weakly on the chosen cloud model. Therefore, either of these models can be used subsequently for further analysis (e.g., optical depth retrieval). The second model depends on fewer parameters and is the simpler of the two; hence, it is more attractive for practical use.

# Conclusion

The basic objective of cloud detection from space is to define the spatial arrangement of individual clouds, both vertically and horizontally. The possibility in getting this detailed information from the high-resolution MISR observations is the purpose of this article.

The suggested approach allows one to determine both the horizontal distribution of cloud pixels, and their geometrical thickness $\Delta h$ from the angular variations of the measured radiances. As a case study, MISR images of small marine cumulus clouds were chosen. The obtained results demonstrate that multiangular MISR data have the potential for measuring individual cloud geometry. However, further testing is needed to better understand the limits and accuracy of the approach. With this aim in mind, we will verify the suggested geometrical thickness retrieval $\Delta h$ with independent data. The retrieved

cloud geometrical properties can serve as a basis for estimating optical ones from additional radiative modeling. The retrievals of cloud optical properties from MISR data will be a subject of our future investigation.

## Acknowledgments

This work was supported by the Office of Biological and Environmental Research of the U.S. Department of Energy as part of the ARM Program and by NASA under contract number 121164 with NASA/Jet Propulsion Laboratory (JPL).

## Corresponding Author

E. I. Kassianov, Evgueni.Kassianov@pnl.gov; (509) 372-6535

## References

Chambers, L., B. A. Wielicki, and K. F. Evans, 1997: Accuracy of the independent pixel approximation for satellite estimates of oceanic boundary layer cloud optical depth. *J. Geophys. Res.*, **102** (D2), 1779-1794.

Han, D., and R. G. Ellingson, 1999: Cumulus cloud formulations for longwave radiation calculations. *J. Atmos. Sci.*, **56**, 837-850.

Minnis, P., P. W. Heck, D. F. Young, C. W. Fairall, and B. J. Snider, 1992: Stratocumulus cloud properties derived from simultaneous satellite and island-based instrumentation during FIRE. *J. Appl. Meteor.*, **31**, 317-339.

Rossow, W., 1989: Measuring cloud properties from space: A review. *J. Climate*, **2**, 201-213.

Rossow, W., F. Mosher, E. Kinsella, A. Arking, M. Desbois, E. Harrison, P. Minnis, E. Ruprecht, G. Seze, C. Simmer, and E. Smith, 1985: ISCCP cloud algorithm intercomparison. *J. Climate Appl. Meteor.*, **24**, 877-903.

Titov, G., 1990: Statistical Description of Radiation Transfer in Clouds. *J. Atmos. Sci.* **47**, 14-38.